Chinese Journal of Mechanical Engineering

ORIGINAL ARTICLE

Open Access

High-resolution Transmission Electron Microscopy Characterization of the Structure of Cu Precipitate in a Thermal-aged Multicomponent Steel

Lizhan Han[1], Qingdong Liu[1,2*] and Jianfeng Gu[1,2]

Abstract

High-dispersed nanoscale Cu precipitates often contribute to extremely high strength due to precipitation hardening, and whereas usually lead to degraded toughness for especially ferritic steels. Hence, it is important to understand the formation behaviors of the Cu precipitates. High-resolution transmission electron microscopy (TEM) is utilized to investigate the structure of Cu precipitates thermally formed in a high-strength low-alloy (HSLA) steel. The Cu precipitates were generally formed from solid solution and at the crystallographic defects such as martensite lath boundaries and dislocations. The Cu precipitates in the same aging condition have various structure of BCC, 9R and FCC, and the structural evolution does not greatly correlate with the actual sizes. The presence of different structures in an individual Cu precipitate is observed, which reflects the structural transformation occurring locally to relax the strain energy. The multiply additions in the steel possibly make the Cu precipitation more complex compared to the binary or the ternary Fe–Cu alloys with Ni or Mn additions. This research gives constructive suggestions on alloying design of Cu-bearing alloy steels.

Keywords: Cu precipitate, High-resolution transmission electron microscopy, Thermal aging, High-strength low-alloy steel

1 Introduction

The nanoscale Cu precipitates often endows alloyed steels with dramatically high strength but simultaneously lead to degraded impact toughness especially at cryogenic temperature [1–3]. The nature of Cu precipitation in α-Fe matrix have been comprehensively investigated in aspect of mutual development of composition, structure and morphology [4]. It has been established that the Cu precipitates contain significant concentration of Fe and are also rich in Ni and Mn at their initial nucleation stage [7]. With the precipitation reaction proceeding, Fe atoms are gradually expelled into the matrix and Ni and Mn tend to segregate at the precipitate/α-Fe boundaries [8, 9]. Meanwhile, the structure of Cu precipitates evolves following a complicated BCC→9R→3R→FCC sequence [10, 11], and the BCC Cu precipitates are considered to be originate from the growth of B2 ordered domains, as reported by Wen et al. [12]. Accompanying the compositional and structural evolution, the morphology of Cu precipitates generally changes from spherical to ellipsoidal to rod-like shape [4, 13]. The transformations in course of Cu precipitation collectively take place in order to reduce the related coherent strain energy, interfacial energy and inherent energy of Cu precipitates.

The structural evolution of Cu precipitates in α-Fe is extremely complex. It is known that the Cu atoms initially experience a coherent precipitation to form a B2 or BCC structure in the BCC α-Fe [14], and then the metastable structures transform to an internally twinned martensitic 9R structure (the stacking sequence of the closely

*Correspondence: qdliu@sjtu.edu.cn
[1] Institute of Materials Modification and Modelling, School of Materials Science and Engineering, Shanghai Jiao Tong University, Shanghai 200240, China
Full list of author information is available at the end of the article

Springer Open

© The Author(s) 2019. This article is distributed under the terms of the Creative Commons Attribution 4.0 International License (http://creativecommons.org/licenses/by/4.0/), which permits unrestricted use, distribution, and reproduction in any medium, provided you give appropriate credit to the original author(s) and the source, provide a link to the Creative Commons license, and indicate if changes were made.

packed planes is ABC/BCA/CAB/A) by the repeated shear of $\{110\}_{\alpha\text{-Fe}}$ planes with an orientation relationship $(011)_{\alpha\text{-Fe}}$ // $(11\text{-}4)_{9R}$, $[1\text{–}11]_{\alpha\text{-Fe}}$ // $[\text{-}110]_{9R}$ [10]. The following possible changes in the 9R structure, including the detwinning of typical twin variants by migration of intervariant (twins) boundary, rotation of closed-packed $(009)_{9R}$ basal planes to align more close to $\{110\}_{\alpha\text{-Fe}}$, and elimination of regular stacking faults on the $(009)_{9R}$ basal planes [15], can produce a more stable 3R structure with non-cubic heavily distorted FCC structure [11]. With subsequent diffusional growth of the 3R structure and the resultant lattice relaxation to minimize total free energy, the expected FCC structure is eventually formed following the Kurdjumov-Sachs orientation [15]. The 9R, 3R and FCC structures are all possibly be with twined or untwined structure, as the untwined 9R and twined 3R or FCC structures were all reported by Feng [16] and Heo et al. [17]. In addition, the critical size of Cu precipitates at which the structural transformation occurs also appear to be different. The complexity of the structural evolution of Cu precipitates is usually ascribed to the differences in the initial compositions and/or the actual heat treatments (tempering or ageing intensity) of the model or multicomponent steels investigated [18–25]. The deformation (stress or strain) and irradiation also prove to efficiently induce or accelerate BCC to 9R transformation [18, 22]. In addition, computational modeling also used to understand the structural and compositional evolution in Fe–Cu-X (X denotes Mn and/or Ni, etc.) systems [26–32], and indicates that the structures of Cu precipitates are greatly influenced by alloying elements.

Hence, the structural development of Cu precipitates is extremely complex and need to be experimentally studied on more extended ferritic steels. The aim of the present work is to provide more information on the structural evolution of Cu precipitates in a thermal-aged multicomponent steel by using high-resolution transmission electron microscopy (HRTEM).

2 Experimental Details

The experimental steel was received from IRIS, Shasteel China with compositions of 0.04 C, 0.24 Si, 0.84 Mn, 1.15 Cu, 1.94 Ni, 0.51 Mo, 0.50 Cr, 0.043 Nb, 0.009 Ti, 0.03 Al, 0.004 N, 0.007 P, and 0.004 S (wt. %) (More see reference [19]). The steel was solution treated at 900 °C for 30 min followed by water-quenching and thermally aged at 500 °C for 16 h when most of Cu precipitates were in overaged conditions. HRTEM observation were performed on a JEOL 2010F (Tokyo, Japan) at 200 kV. Although it has been found that the characteristic 9R "herring-bone" fringe pattern can only be well imaged with the beam direction closely parallel to a $<111>_{\alpha\text{-Fe}}$ direction [11], most micrographs in this paper were alternatively taken along a $<001>_{\alpha\text{-Fe}}$ direction in order to give different appearances of the Cu precipitates. Thin foil specimens were prepared by mechanically grinding sample slices to 80-μm thick and twin-jet electropolishing in a mixture of 90% alcohol and 10% perchloric acid at − 30 °C under 50 V.

3 Results and Discussion

Figure 1a shows a HRTEM micrograph taken along a $[001]_{\alpha\text{-Fe}}$ direction of the sample aged at 500 °C for 16 h. Several nanoscale Cu precipitates can be recognized by the strain field contrast (black domains marked by circle) arose from lattice distortion and by the somewhat weak fringe contrast (marked by arrow) where the atomic columns are mostly ill-arranged. These precipitates are formed in association with linear dislocation as they generally distributed in an arc curve (highlighted by dash line), which is consistent with the APT observation of Cu precipitates in a similar steel [19]. The Fast Fourier transform (FFT) conducted on two representative Cu precipitates (labeled A and B, respectively) embedded in α-Fe in the dashed square in Figure 1a shows that the diffraction spots from the precipitates exactly overlap with those from α-Fe matrix, as shown in Figure 1b, which indicates the identical BCC structure and the absolute coherency of the Cu precipitates and α-Fe matrix. Faint extra weak spots (marked by arrows) along $\mathbf{g}=[020]_{\alpha\text{-Fe}}$ are responding to the anomalous fringe spacings in precipitate B, as discussed later. However, no evidence of the formation of B2 ordered domains reported by Wen et al. [12] is found from the FFT pattern, although the image here is also taken along the $[001]_{\alpha\text{-Fe}}$ direction and the steels used are similarly alloyed with multiple elements. In a BCC Cu and B2-NiAl precipitation strengthened ferritic steel, Kapoor et al. [20] found that the B2 ordered diffraction become distinct only when the B2-NiAl precipitates have an average radius of 4.28 ± 1.47 nm (obtained by APT analysis) after at least aging at 550 °C for 10 h. The B2 ordered diffraction is seemingly too weak to be detectable for the nanoscale features using the HRTEM, since the imaging mechanism and the working conditions (such as voltage employed) of HRTEM are both also different from that of the HAADF-STEM.

The corresponding inverse Fast Fourier transform (IFFT) of Figure 1b presents a more distinct atomic structure of the Cu precipitates, as shown in Figure 1c. In precipitate A, the 'black' strain contrast possibly is associated with the compositional fluctuation, since the nanoscale bcc Cu precipitates are thought to contain high concentrations of Fe, Ni and Mn [7]. Other studies [10–12] on relatively simply Fe–Cu or Fe–Cu–Ni model alloys showed that the bcc Cu precipitates, which had a structure and lattice parameters identical to α-Fe, were not

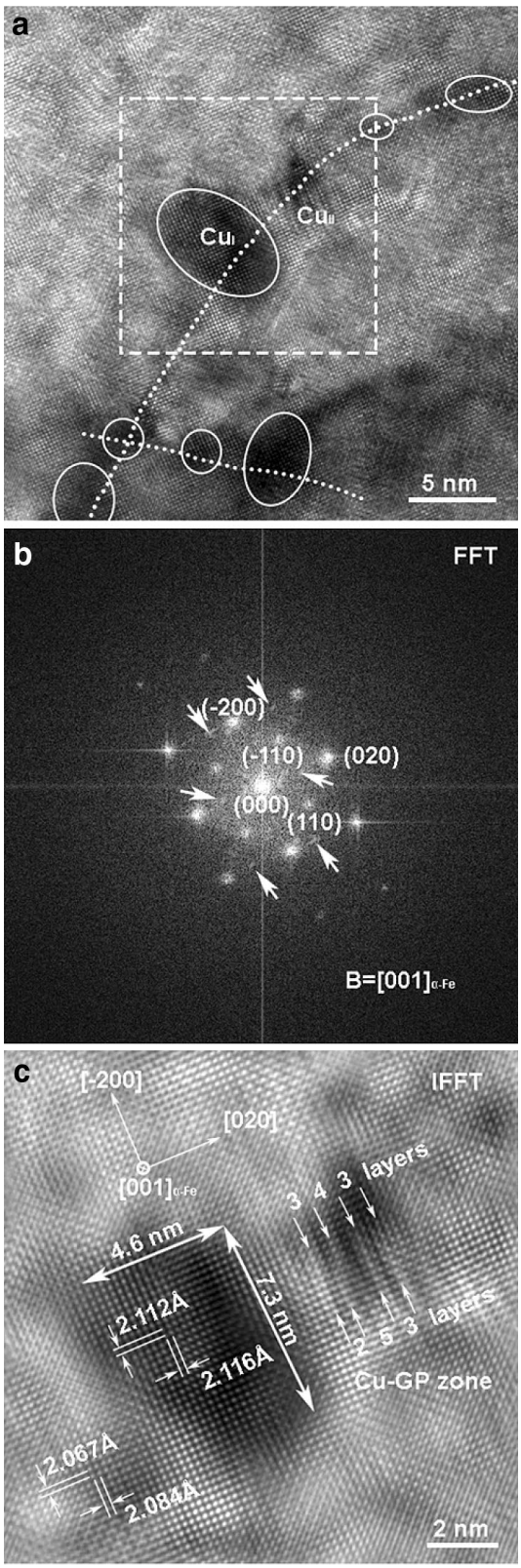

Figure 1 **a** HRTEM image of BCC Cu precipitates formed on dislocations and in α-Fe matrix; **b** FFT pattern of the region in dash square in **a**; **c** IFFT image of **b**, showing two Cu-rich precipitates with different morphology

readily to be imaged by using the phase contrast method of HRTEM. The precipitate/matrix interface is therefore roughly distinguished by the strain contrast and the precipitate A is found to have a size approximately 6 nm in diameter (average of major and minor axis values). The (020)/(-200) interplanar spacings of the precipitate and α-Fe are carefully measured to be 2.116 Å/ 2.112 Å and 2.084 Å/2.067 Å, respectively, which gives rise to slight lattice deviation along [020] and [-200] directions. The small misfit inevitably induced coherent strain energy, which may serve as main driving force for bcc to 9R martensitic transformation.

In precipitate B, the appearance of irregular striations (marked by arrows) along the $[-200]_{\alpha\text{-Fe}}$ direction, which correspond to the weak diffraction spots between g_{000} and g_{020} spots, manifests the distorted lattices in the precipitate and resultant 'black' strain contrast, as shown Figure 1c. One possibility that the anisotropic atoms of Cu segregate at given lattice planes of α-Fe can account for the anomalous atomic structure of the precipitate, which is consistent with the observation by Xu at al. [21] in a thermal-aged reactor pressure vessel (RPV) model steel with enhanced Cu content. The Cu segregation undoubtedly induces significant lattice misfit of α-Fe, which in turn impede the segregation occurring on continual lattice planes and, the Cu atoms hence tend to periodically replace the Fe atoms. The Cu segregation seems to be rather irregular here and its periodicity generally possesses 2–5 column spacings. However, as observed by Xu et al., the segregated Cu atoms can be regularly arranged every three sets of $\{110\}_{\alpha\text{-Fe}}$ planes and the periodical spacing is measured to be 0.6 nm, which is right consistent with the spacing of the herring-bone fringes of 9R structure [10]. The anomalous atom arrangement in the present nanoscale Cu precipitate seems to represent an earlier nucleation stage. Moreover, note that the $[001]_{\alpha\text{-Fe}}$ incidence direction may also cause the different appearance of Cu precipitate in HRTEM. The Cu segregation at certain lattice planes of α-Fe preceding to the Cu precipitation is similar to the formation of G.P. zone in some Al alloys, which are both energetically favorable. Overall, regular segregation of Cu atom perceivably occurs periodically with the Cu precipitation proceeding, leading to the development of the BCC structured (such as precipitate A) and further the 9R structured Cu precipitates.

Figure 2a shows a HRTEM micrograph and Figure 2b the corresponding Fast Fourier Transform pattern with index illustration taken along a $[001]_{\alpha\text{-Fe}}$ direction of the sample aged at 500 °C for 16 h. A straight zone with distinct "black" strain contrast where the atoms are seriously ill arranged and the lattice is significant distorted indicates the appearance of a martensite lath

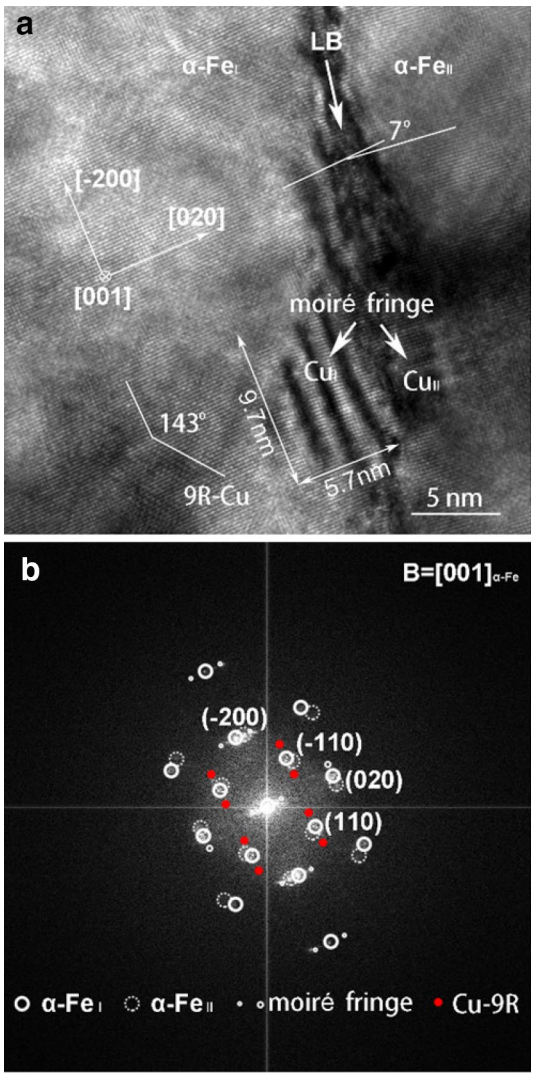

Figure 2 **a** HRTEM image of Cu precipitates formed at a martensite lath boundary and in α-Fe matrix; **b** FFT pattern of **a**, showing the presence of 9R Cu precipitate

boundary (LB), which divides the whole ferritic matrix into α-Fe_I and α-Fe_{II} crystals. The angular deviation of the two α-Fe crystals is measured to be approximately 7°, which is also consistent with the low angle martensite LBs. Two adjacent Cu precipitates (labeled Cu_I and Cu_{II} detected in α-Fe_I and α-Fe_{II}, respectively) at the LB exhibit evident Moiré fringes arising from the lattice overlap, which also brings about extra diffraction spots close to the $g_{<200>α-Fe}$ spots, as shown in Figure 2b. The fringes are almost parallel to the $[-200]_{α-FeI}$ and $[020]_{α-FeII}$, respectively. The Moiré fringes, the intensity of which is related to the in incidence direction as discussed followed, make the fine structure of the Cu precipitates difficult directly imaged for further analysis. Compared to that formed on the dislocation (Figure 1), the Cu precipitates formed in association with LBs generally have relatively larger sizes (approximately 7.8 nm for Cu_{II}), which is possibly attributed to faster diffusion of related solutes along LBs than dislocations. The Cu precipitates are thought to have a possible 9R structure as they are listed in the size range of 9R structure but which cannot be well established. A Cu precipitate with 9R structure, however, is easily recognized in α-Fe_I containing only two twin-related variant segments. The characteristic herring-bone fringe patterns are not observed, that is, there is no stacking fault every three closely packed planes in the adjacent twin segments, but in which the striations become evident and their angles are approximately 143°. The $(-1-14)_{9R}$ mirror boundary lies parallel to $<110>_{α-FeI}$, as shown by extra diffraction spots in Figure 2b. It seems that it is not necessary to form SF in 9R structure, because the strain energy between 9R Cu and the a-matrix can be sufficiently reduced by formation of $(114)_{9R}$ twins. In addition, it is suggested the typical 9R structure is indeed not easily detected with $[001]_{α-Fe}$ direction [10, 11].

Figure 3 gives HRTEM analysis of several Cu precipitates in the same sample as that in Figures 1 and 2. The micrograph in Figure 3a taken along a $[001]_{α-Fe}$ direction shows the presence of Cu precipitates (labeled Cu_I and Cu_{II}) recognized from the evident moiré fringes. The general FFT patterns from the two Cu precipitates in the selected zones (dash square) are somewhat different, corresponding to their observed different configuration as discussed below. However, the FFT patterns from Cu_I and Cu_{II} are generally identical to that from α-Fe because the main diffraction spots from the precipitates may overlap with the fundamental diffraction from α-Fe, except for the presence of extra weak diffraction spots corresponding to the complex structure of the two Cu precipitates after careful examination. In addition, three selected regions marked A, B and C (dash circle) show less distinct moiré fringes. In these regions, the fringes generally lie parallel to $[020]_{α-Fe}$ (regions A and B) or just slightly deviate from $[-110]_{α-Fe}$ direction with an angle of approximately 8° (Region C). It is interesting to see that the moiré fringes changes in appearance as the bean orientation varies approximately 5°, as shown in Figure 3b. At the same time, the corresponding diffraction spots arising from these faint moiré fringes slightly move around after carefully conducting the FFT on these regions. The Cu precipitates possibly have a BCC structure like those shown in Figure 1. However, the moiré fringe and their diffraction spots are not from the Cu precipitates themselves but thought to be formed by overlap of the $(020)_{α-Fe}$ with $(020)_{BCC-Cu}$ (region A and B) and $(-110)_{BCC-Cu}$ (region C). The deviation of moiré fringes

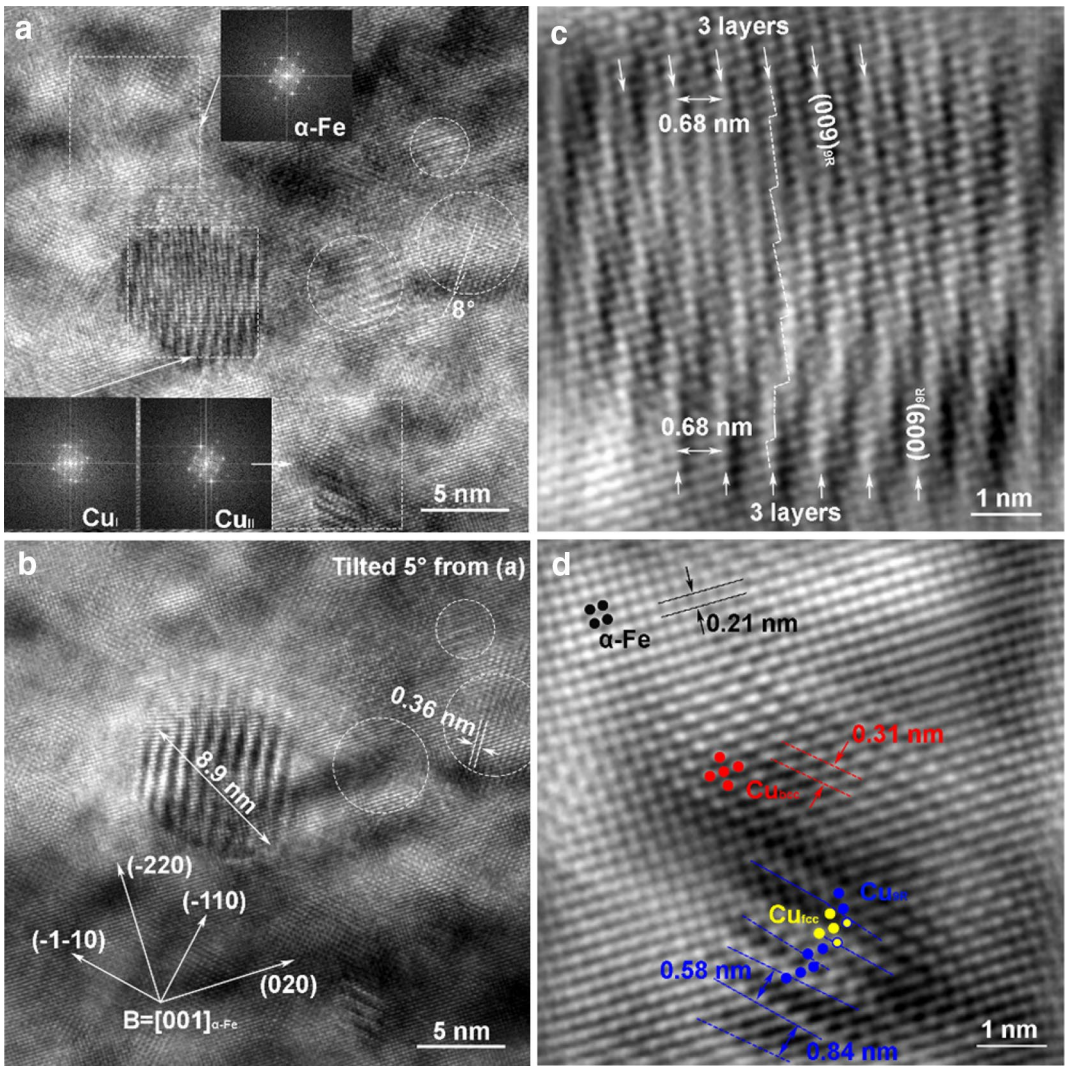

Figure 3 **a** HRTEM image of Cu precipitates formed in α-Fe matrix; **b** HRTEM image with 5o tilted from **a**; **c**, **d** IFFT images of selected Cu_I and Cu_{II} in **a**, indicating the complex structure of Cu precipitates

from $[-110]_{\alpha\text{-Fe}}$ direction in region C indicates a slightly angular rotation of the BCC Cu precipitate to α-Fe, which is considered to facilitate the stress relaxation during BCC to 9R transformation.

Figure 3c and d give the atomic structure of the Cu_I and Cu_{II}, respectively, by conducing IFFT on the corresponding FFT patterns in Figure 3a. The atomic columns are not readily distinguished with the interference from strain field and moiré fringe contrast. The Cu_I has a heavily distorted untwined 9R structure. The perfect untwined 9R structure was previously found during aging of a Fe-3Si-2Cu alloy [17], but such irregular precipitate of Cu_I with significantly distorted lattice with SF were not reported before. The distorted structure of the precipitates may be ascribed to the complex compositional fluctuation with Ni and Mn segregation and partitioning between α-Fe and precipitates during their growth and coarsening. In addition, the distortion seems to be necessary in the formation of 9R precipitates. Random SF is inevitably generated to meet the invariant plane condition during the BCC-to-9R transformation. The Cu_{II} is a non-spherical 9R precipitate contains single variants without the twin (intervariant) mirror plane. The 9R stacking sequence is randomly destroyed and the fringes appear to be not uniformly distributed, equal to 2–5 times the $(009)_{9R}$ close-packed plane spacing. There are several regions with different atom arrangement that indicates the coexisting of different structures of α-Fe,

BCC Cu, 9R Cu and FCC Cu by measuring the given lattice spacing. However, no direct evidence for these coexisting structure could be obtained from the diffraction patterns in Figure 3a taken from this region, as the precipitate reflections arising from different structures are extremely weak and their proximity to matrix reflection. It is suggested that the multiply structural transition of the Cu precipitate can occur via atomic relaxation in an individual precipitate, leading to the complex structure of the Cu precipitates. In addition, the transformation occurs at atomic scale and seems to be independent of the precipitate size. It is generally recognized that the structure of Cu precipitates roughly depends on their actual size. The exceptional case herein is possibly attributed to the systematic effect of multiple solute additions especially Ni and Mn, etc. which greatly influence the nucleation and growth of the Cu precipitates.

Figure 4 shows HRTEM analysis of a selected Cu precipitate with a relatively large size. The precipitate in Figure 4a taken along a [111] $_{\alpha\text{-Fe}}$ direction have a FCC structure, as shown by the FFT image of Figure 4a in Figure 4b. Close observation of the diffraction patterns reveals the presence of faint extra spots marked by the blue squares, which is considered to correspond to the faults in the FCC structure. IFFT image in Figure 4c of the region in the white square in Figure 4a shows the fine structure of the precipitate adjacent to the matrix. Distinct faults are observed with irregular crystal lattices, as marked by blue lines. EDS analysis in Figure 4d shows the presence of additional Ni and Mn as well as the carbide-forming elements Mo and Nb in the precipitate, which is possibly responded for the formation of faults even at the later coarsening stage. It seems that active diffusion of these heteroatoms facilities the relaxation of strain

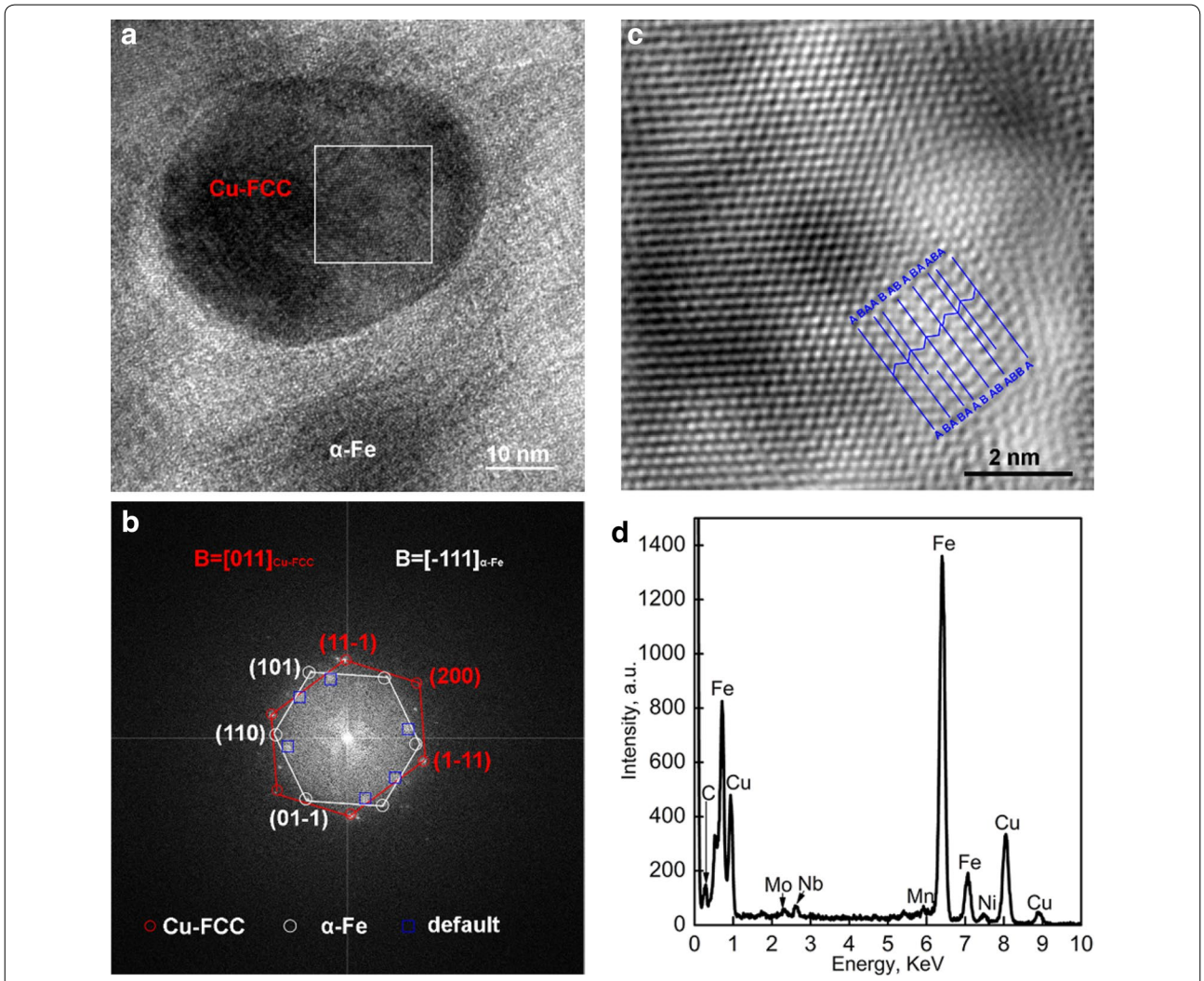

Figure 4 **a** HRTEM image of a coarsened FCC Cu precipitate; **b** FFT pattern of whole image **a**; **c** IFFT image of the region in white square in **a**; **d** EDS analysis of the precipitate

energy by forming faults during the formation of FCC structure. Therefore, the structural evolution of Cu precipitates seems to be more complex in multicomponent steels than that in binary or the ternary Fe–Cu alloys with merely Ni or Mn additions.

4 Conclusions

The Cu precipitates in a high-strength low-alloy steel isothermally aged at 500 °C for different time are characterized by using high-resolution transmission electron microscopy. The following conclusions are drawn from this study.

(1) The Cu precipitates preferentially nucleate at crystallographic defects such as dislocations and martensite LBs.
(2) Although imaged in the same aging condition, the Cu precipitates have multiple structure of BCC, 9R and FCC and vary in a wide size region. However, the structural evolution does not greatly correlate with the actual sizes.
(3) The presence of different structures can exist in an individual Cu precipitate, reflecting the local occurrence structural transformation to relax the strain energy.
(4) The complex Cu precipitation compared to that in the binary or the ternary Fe–Cu alloys with merely Ni or Mn additions is attributed to the multiply additions in the multicomponent steel.

Authors' Contributions
QL and JG as in charge of the whole trial; LH wrote the manuscript; QL and LH assisted with sampling and laboratory analyses. All authors read and approved the final manuscript.

Authors' Information
Lizhan Han, born in 1970, is currently an assistant researcher at *School of Materials Science and Engineering, Shanghai Jiao Tong University, China*. He received his doctoral degree from *Shanghai Jiao Tong University, China*, in 2010. His research interests include heat treatment of heavy steel forges.

Qingdong Liu, born in 1982, is currently an assistant researcher at *School of Materials Science and Engineering, Shanghai Jiao Tong University, China*. He received his doctoral degree from *Shanghai University, China*, in 2013.

Jianfeng Gu, born in 1970, is currently a professor at *School of Materials Science and Engineering, Shanghai Jiao Tong University, China*.

Acknowledgements
The authors sincerely thanks to Dr. Jianchao Peng of Shanghai University for his critical discussion on TEM analysis and reading during manuscript preparation.

Competing Interests
The authors declare that they have no competing interests.

Funding
Supported by Startup Fund for Youngman Research at SJTU (SFYR at SJTU), National Basic Research Program of China (Grant No. 2011CB012904), and China Postdoctoral Science Foundation (Grant No. 2013M541517).

Author Details
[1] Institute of Materials Modification and Modelling, School of Materials Science and Engineering, Shanghai Jiao Tong University, Shanghai 200240, China.
[2] Collaborative Innovation Center for Advanced Ship and Deep-Sea Exploration, Shanghai Jiao Tong University, Shanghai 200240, China.

Received: 1 April 2019 Revised: 24 June 2019 Accepted: 25 September 2019
Published online: 11 October 2019

References

[1] A Saha, J Jung, G B Olson. Prototype evaluation of transformation toughened blast resistant naval hull steels: Part II. *J. Computer-Aided Mater. Des.*, 2007, 14: 201-233.
[2] M D Mulholland, D N Seidman. Nanoscale co-precipitation and mechanical properties of a high-strength low-carbon steel. *Acta Mater.*, 2011, 59: 1881-1897.
[3] Q D Liu, H M Wen, H Zhang, et al. Effect of multistage heat treatment on microstructure and mechanical properties of a high-strength low-alloy steel. *Metall. Mater. Trans. A*, 2016, 47A: 1960-1974.
[4] R P Kolli, D N Seidman. The temporal evolution of the decomposition of a concentrated multicomponent Fe–Cu-based steel. *Acta Mater.*, 2008, 56: 2073-2088.
[5] J Takahashi, K Kawakami, Y Kobayashi. Consideration of particle- strengthening mechanism of copper-precipitation-strengthened steels by atom probe tomography analysis. *Mater. Sci. Eng. A*, 2012, 535: 144-152.
[6] Q D Liu, Y H Chen, C W Li, et al. Compositional variants of Cu-rich precipitate in thermally aged ferritic steel. *Acta Metall. Sin. (English Letters)*, 2018, 31: 465-470.
[7] M Schober, E Eidenberger, H Leitner, et al. A critical consideration of magnetism and composition of (bcc) Cu precipitates in (bcc) Fe. *Appl. Phys. A*, 2010, 99: 697-704.
[8] D Isheim, M S Gagliano, M E Fine, et al. Interfacial segregation at Cu-rich precipitates in a high-strength low-carbon steel studied on a sub-nanometer scale. *Acta Mater.*, 2006, 54: 841-849.
[9] R P Kolli, Z Mao, D N Seidman, et al. Identification of a $Ni_{0.5}(Al_{0.5-x}Mn_x)$ B2 phase at the heterophase interfaces of Cu-rich precipitates in an α-Fe matrix. *Appl. Phys. Lett.*, 2007, 91: 241903.
[10] P J Othen, M L Jenkins, G D W Smith, et al. Transmission electron microscope investigations of the structure of copper precipitates in thermally-aged Fe–Cu and Fe–Cu-Ni. *Philos. Mag. Lett.*, 1991, 64: 383-391.
[11] P J Othen, M L Jenkins, G D W Smith. High-resolution electron microscopy studies of the structure of Cu precipitates in α-Fe. *Philos. Mag.*, 1994, 70A: 1-24.
[12] Y R Wen, A Hirata, Z W Zhang, et al. Microstructure characterization of Cu-rich nanoprecipitates in a Fe-2.5 Cu-1.5 Mn-40 Ni-1.0 Al multicomponent ferritic alloy. *Acta Mater.*, 2013, 61: 2133-2147.
[13] R Monzen, K Takada, C Watanabe. Coarsening of spherical Cu particles in an α-Fe matrix. *ISIJ Int.*, 2004, 44: 442-444.
[14] S Pizzini, K J Roberts, W J Phythian, et al. A fluorescence EXAFS study of the structure of copper-rich precipitates in Fe–Cu and Fe–Cu-Ni alloys. *Philos. Mag. Lett.*, 1990, 61: 223-229.
[15] R Monzen, M Iguchi, M L Jenkins. Structural changes of 9R copper precipitates in an aged Fe–Cu alloy. *Philos. Mag. Lett.*, 2000, 80: 137-148.
[16] L Feng. *Crystal structure evolution and deformation characteristics of Cu-rich nano-phase in RPV model steels*. Shanghai University, China, 2014.
[17] Y U Heo, Y K Kim, J S Kim, et al. Phase transformation of Cu precipitates from bcc to fcc in Fe-3Si-2Cu alloy. *Acta Mater.*, 2013, 61: 519-528.
[18] S Lozano-perez, M L Jenkins, J M Titchmarsh. Evidence of deformation-induced transformation of Cu-rich precipitates in and aged FeCu alloy. *Philos. Mag. Lett.*, 2006, 86: 367-374.
[19] Q D Liu, S J Zhao. Cu precipitation on dislocations and interfaces in quench-aged steel. *MRS Communi.*, 2012, 2: 127-132.
[20] M Kapoor, D Isheim, G Ghosh, et al. Aging characteristics and mechanical properties of 1600MPa body-centered cubic Cu and B2-NiAl precipitation-strengthened ferritic steel. *Acta Mater.*, 2014, 73: 56-74.
[21] G Xu, D F Chu, L L Cai, et al. Investigation on the precipitation and structural evolution of Cu-rich nanophase in RPV model steel. *Acta Metall. Sin.*, 2011, 47: 905-911. (in Chinese)

[22] X M Bai, H Ke, Y Zhang, et al. Modeling copper precipitation hardening and embrittlement in a dilute Fe-0.3 at% Cu alloy under neutron irradiation. *J. Nucl. Mater.*, 2017, 495: 442-454.
[23] Q D Liu, J F Gu. Hierarchical Cu precipitation in lamellated steel after multistage heat treatment. *Philosophical Magazine*, 2017, 97: 2361-2374
[24] Q D Liu, C W Li, J F Gu. Interactive formation of Cu-rich precipitate, reverted austenite, and alloyed carbide during partial austenite reversion treatment for high-strength low-alloy steel. *Journal of Materials Research*, 2017, 32: 2325-2334.
[25] Q D Liu, J F Gu, C W Li. Regulation of Cu precipitation by intercritical tempering in a HSLA steel. *J. Mater. Res.*, 2014, 29: 950-958.
[26] S Kajiwara. Theoretical analysis of the crystallography of the bcc to FCT martensitic transformation. *The Japan Society of Applied Physics*, 1976, 17(7): 435-446.
[27] L Qin, A Redermeier, C Dellago, et al. Rigid-lattice Monte Carlo study of nucleation kinetics in dilute bcc Fe–Cu alloys using statistical sampling techniques. *Acta Mater.*, 2018, 159: 429-438
[28] J M Zhu, T L Zhang, Y Yang, et al. Phase field study of the copper precipitation in Fe–Cu alloy. *Acta Mater.*, 2019, 166: 560-571.
[29] G Stechauner, E Kozeschnik. Thermo-kinetic modeling of Cu precipitation in α-Fe. *Acta Mater.*, 2005, 100: 135-146
[30] S P Shu, P B Wells, N Almirall, et al. Thermodynamics and kinetics of core-shell versus appendage co-precipitation morphologies: An example in the Fe–Cu-Mn-Ni-Si system. *Acta Mater.*, 2018, 157: 298-306.
[31] D Molnar, R Mukherjee, A Choudhury, et al. Multiscale simulations on the coarsening of Cu-rich precipitates in α-Fe using kinetic Monte Carlo, molecular dynamics, and phase-field simulations. *Acta Mater.*, 2016, 60(20): 15-36.
[32] P Erhart, B Sadigh. Low-temperature criticality of martensitic transformations of Cu nanoprecipitates in α-Fe. *Phys. Rev. Lett.*, 2013, 111(2): 025701.

Submit your manuscript to a SpringerOpen journal and benefit from:

► Convenient online submission
► Rigorous peer review
► Open access: articles freely available online
► High visibility within the field
► Retaining the copyright to your article

Submit your next manuscript at ► springeropen.com